Combinatorial Approaches to Understanding Polytypism in III–V Nanowires

Jonas Johansson,[*,†] Jessica Bolinsson,[†] Martin Ek,[‡] Philippe Caroff,[§] and Kimberly A. Dick[†,‡]

[†]Solid State Physics, Lund University, Box 118, S-22100 Lund, Sweden, [‡]Polymer & Materials Chemistry, Lund University, Box 124, S-22100 Lund, Sweden, and [§]Institut d'Electronique de Microélectronique et de Nanotechnologie, UMR CNRS 8520, Avenue Poincaré, B.P. 60069, 59652 Villeneuve d'Ascq, France

ABSTRACT

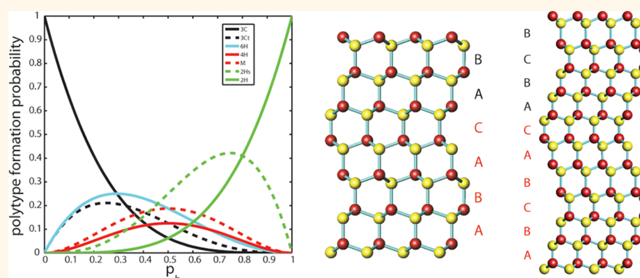

Polytypism in III–V semiconductor nanowires is a topic that has received considerable attention in recent years. Achieving a pure nanowire crystal phase requires well-controlled and advanced parameter tuning for most III–V materials. Additionally, the new and unusual phases sometimes observed may present unique material properties if they can be controllably fabricated. With the prospect of using nanowires in applications within several different fields (including electronics, photonics, and life science), theoretical models are necessary to explain experimental trends and to attain a high level of crystal phase control. At present, there is no theoretical model (or combination of models) that fully explains how and why nanowire crystal structures commonly include several different polytypes. Here we use combinatorics and interlayer interactions to include higher order polytypes (4H and 6H) with the aim to explain nanowire crystal structure beyond the well-investigated zinc blende–wurtzite polytypism. Predictions from our theoretical models compare well with experimental results.

KEYWORDS: nanowires · polytypism · III–V materials · combinatorics · ANNNI model

III–V semiconductor nanowires[1–5] are currently being investigated for a wide range of applications in electronics,[6] photonics,[7] and life sciences.[8] Many of these applications require a high crystal quality, since the crystalline properties determine to a great extent the electronic and optical properties.[9,10] In bulk, all III–V materials, except the nitrides, crystallize in the zinc blende structure, or 3C using the Ramsdell notation.[11] However, nanowires fabricated at arbitrary conditions typically exhibit a highly irregular crystal structure, which can be described as zinc blende with a high density of planar defects. If these defects appear consecutively, the resulting crystal structure will be dominated by wurtzite (2H). If the planar defects are more sparsely distributed, the resulting crystal structure can be described as 3C with lamellar twinning.[12]

In the ⟨111⟩B growth direction, preferred for nanowires, these structures differ only in the stacking sequence of the bilayers, with a repeating ABC sequence for 3C and an AB sequence for 2H (with the lettering indicating the relative positions of the bilayers; see Figure 1a and b). Crystal structures that differ only in the stacking sequence are denoted polytypes. In several materials systems, segments of polytypes with longer repeating periods (4H and 6H) have also been observed.[13–17] These are characterized by the stacking sequences ABAC and ABCBAC, respectively (Figure 1c and d). In addition there are a few reports of periodically twinned nanowires (also referred to as twinning superlattices or twin plane superlattices),[18–20] which we note can be regarded as nH polytypes, where n is the number of bilayers in the smallest repeating stacking unit.[21]

A general understanding of the intrinsic cause of this polytypism in nanowires has been developed in recent years. Classical nucleation theory is used to explain the growth temperature dependence of the density of twin planes,[22] and Glas *et al.* have shown that the formation of 2H can be favorable during nanowire growth at high supersaturation,[23] given that the relevant surface energies are lower than for 3C.[23,24]

The primary limitation of current models based on classical nucleation theory is that they typically determine nucleation probabilities for only single layers and directly equate these probabilities to fractions of 3C and 2H. However, without considering the possible sequences in which these layers

* Address correspondence to jonas.johansson@ftf.lth.se.

Received for review April 4, 2012 and accepted June 9, 2012.

Published online June 10, 2012
10.1021/nn301477x

© 2012 American Chemical Society

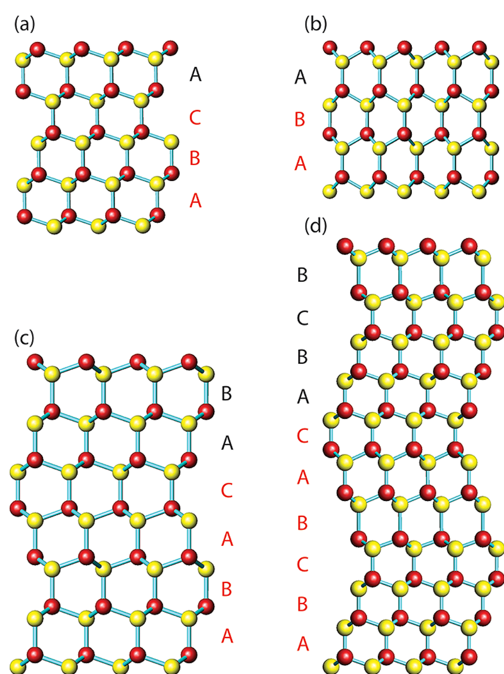

Figure 1. Atomic models of the crystal structure of the polytypes (a) 3C, (b) 2H, (c) 4H, and (d) 6H, including their respective stacking sequences. Representations of the shortest repeating stacking unit for each polytype are highlighted in red.

can form, it is impossible to explain higher order polytypes such as 4H and 6H. The purpose of this investigation is to explain polytypism in nanowires including higher order polytypes using combinatorics, which explicitly considers stacking sequences. That is, our modeling goes far beyond the well-investigated 3C−2H (zinc blende−wurtzite) polytypism.

We first discuss the limits of polytypism in nanowires based on a purely combinatorial model, that is, with more or less random stacking. Following this, we introduce an Ising model for interlayer interaction, to account for the extended single-crystalline segments observed in many nanowire systems. The results suggest that the 4H polytype dominates in a small interval of intermediate supersaturations, below which 3C is stable and above, 2H. Thus, with our approaches we cover the full spectrum: from random stacking to parameter-controlled stacking with long-range order. We show that our theoretical results agree well with experimental observations, both our own and from the literature.

RESULTS AND DISCUSSION

We start by performing combinatorial analysis of the formation probabilities of specific polytype segments. The only input to the model is the two probabilities p_c and p_h, where p_c is the probability of forming a layer on two underlying layers where all three layers are dissimilar, for example A-on-BC or B-on-CA (cubic stacking). The probability p_h is the probability of forming

TABLE 1. List of All the 32 Possible Stacking Sequences Containing Six Layers Starting with A[a]

stacking sequence	polytype	factor
ABABAB	2H	p_h^4
ABABAC	2Hs	$p_c p_h^3$
ABABCA	M	$p_c^2 p_h^2$
ABABCB	2Hs	$p_c p_h^3$
ABACAB	4H	$p_c^2 p_h^2$
ABACAC	2Hs	$p_c p_h^3$
ABACBA	3Ct	$p_c^3 p_h$
ABACBC	6H	$p_c^2 p_h^2$
ABCABA	3Ct	$p_c^3 p_h$
ABCABC	3C	p_c^4
ABCACA	M	$p_c^2 p_h^2$
ABCACB	6H	$p_c^3 p_h$
ABCBAB	4H	$p_c^2 p_h^2$
ABCBAC	6H	$p_c^3 p_h$
ABCBCA	M	$p_c^2 p_h^2$
ABCBCB	2Hs	$p_c p_h^3$
ACABAB	2Hs	$p_c p_h^3$
ACABAC	4H	$p_c^2 p_h^2$
ACABCA	3Ct	$p_c^3 p_h$
ACABCB	6H	$p_c^2 p_h^2$
ACACAB	2Hs	$p_c p_h^3$
ACACAC	2H	p_h^4
ACACBA	M	$p_c^2 p_h^2$
ACACBC	2Hs	$p_c p_h^3$
ACBABC	6H	$p_c^3 p_h$
ACBACB	3C	p_c^4
ACBABA	M	$p_c^2 p_h^2$
ACBACA	3Ct	$p_c^3 p_h$
ACBCAB	6H	$p_c^3 p_h$
ACBCBA	M	$p_c^2 p_h^2$
ACBCAC	4H	$p_c^2 p_h^2$
ACBCBC	2Hs	$p_c p_h^3$

[a] Each stacking sequence is identified as a polytype and assigned a formation probability factor.

a layer that is similar to its next nearest neighbor, for instance A-on-BA or C-on-AC (hexagonal stacking). In this model the only effective interaction is with the next nearest layer, so that p_c may be identified as the nucleation probability of an ordinary layer in 3C, whereas p_h can be identified as the nucleation probability of a twin plane in 3C.[25,26] In the Methods section we describe the parameter dependence of these nucleation probabilities.

In order to include polytypes up to 6H, a combinatorial analysis of stacking sequences at least six layers thick is required. There are in total 96 different sequences that consist of precisely six layers. These can be grouped in three equivalent groups of 32 sequences each. Thus, it is enough to analyze one of these groups, and we choose the one with sequences starting on A. In the left column of Table 1, all these stacking sequences are listed. In the middle column the associated polytypes are shown, and the third column shows the associated probability factor. The hexagonality, which is the fraction of hexagonal

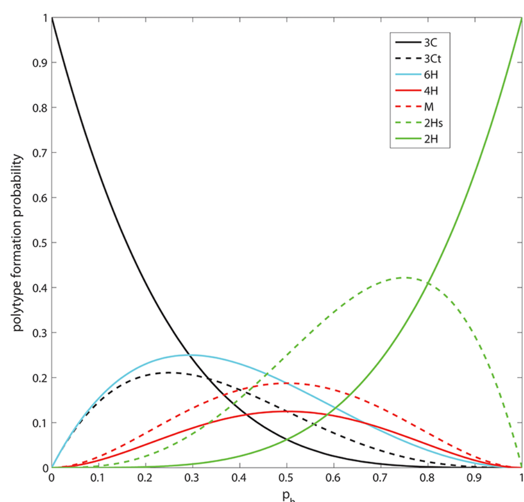

Figure 2. Polytype formation probabilities for different polytypes up to 6H as a function of the hexagonal stacking probability.

stacking in a polytype, can be calculated as the number of p_h's divided by the total number of p_h's and p_c's appearing in the probability factors for each polytype. We note that we recover the known hexagonalities of 0% for 3C, 33.3% for 6H, 50% for 4H, and 100% for 2H.[27]

Some of the stacking sequences in Table 1 do not belong to any one of the common polytypes 3C, 6H, 4H, and 2H. These arise from the truncation of the stacking sequence after exactly six layers and are labeled as 3Ct, 2Hs, and M. The phase 3Ct, which has hexagonality 25%, can most easily be described as heavily twinned 3C, whereas 2Hs, which has hexagonality 75%, can correspondingly be described as 2H with a high density of stacking faults. The M phase is a mixed phase with hexagonality 50%.

We will now express the formation probabilities of the polytypes in Table 1. We note that the sum of all the probability factors is 2, or explicitly, $2(p_c + p_h)^4 = 2$. The formation probabilities of the different polytypes read, in order of increasing hexagonality:

$$\begin{aligned} p_{3C} &= p_c^4 \\ p_{3Ct} &= 2p_c^3 p_h \\ p_{6H} &= p_c^2 p_h^2 + 2p_c^3 p_h \\ p_{4H} &= 2p_c^2 p_h^2 \\ p_M &= 3p_c^2 p_h^2 \\ p_{2Hs} &= 4p_c p_h^3 \\ p_{2H} &= p_h^4 \end{aligned} \tag{1}$$

In Figure 2, we plot the probabilities in eq 1 as a function of p_h, noting that $p_c = 1 - p_h$. For low values of p_h, the 3C polytype dominates, whereas for intermediate values 6H dominates. For higher p_h, the 2Hs polytype dominates, and when p_h exceeds 0.8, the 2H polytype finally dominates. The other polytypes indicated in the graph in Figure 2 never dominate. Although the 4H polytype and the disordered M phase have the same hexagonality, the 4H is always less probable than the M phase. It is noteworthy that besides the 3C and 2H polytypes, the other polytypes have a quite small maximum formation probability.

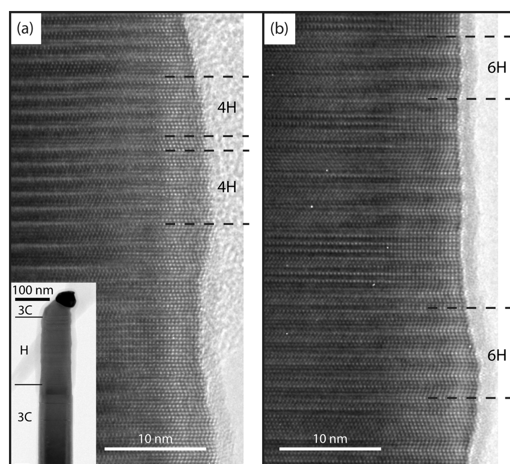

Figure 3. HRTEM images along the ⟨1−10⟩ zone axis of gold particle seeded GaAs nanowires grown with MOVPE at (a) 630 °C and (b) 690 °C with segments of 4H and 6H indicated. The inset shows an overview where the region grown at elevated temperature (630 and 690 °C) and containing a more or less random crystal structure containing 4H and 6H and a high density of planar defects is indicated with H.

Depending on how close to 1 either p_h or p_c is, it is possible to form a (close to) defect-free 2H or 3C crystal structure. However, only when p_h and p_c are significantly different ($p_h > 0.84$ or $p_h < 0.16$) are the formation probabilities of 2H or 3C above 1/2. If neither 2H nor 3C is dominating ($p_h \approx p_c \approx 0.50$), our analysis predicts a 2H-like structure with a high density of stacking faults and possibly short inclusions of other polytypes. The model also predicts that it should be more difficult to get pure 2H than 3C due to the dominance of the 2Hs polytype. It should be noted that 2Hs dominates simply due to its high degeneracy compared to the other stacking sequences (eight pathways lead to 2Hs, two pathways to 3C and to 2H, four pathways to 4H, and six pathways to 6H; see Table 1). This is an interesting finding, as intuitively one would expect that nanowires possessing a mainly 2H-like crystal structure with a lot of stacking faults and very little 3C were grown under conditions where the probability for hexagonal stacking is higher than the one for cubic stacking. Our combinatorial analysis shows the contrary: this situation can also occur when $p_h \approx p_c \approx 0.50$ as an effect of the degeneracy of the different types of stacking sequences.

We now turn to discuss experimental observations in view of the combinatorial analysis outlined above. In Figure 3 we show high-resolution transmission microscopy (HRTEM) images of parts of gold-seeded GaAs nanowires grown with metal organic vapor phase epitaxy (MOVPE) at (a) 630 °C and (b) 690 °C. The inset in (a) shows an overview of a corresponding nanowire. The nanowires in (a) contain on average 7% 4H and 3% 6H, while the nanowires in (b) contain 4% 4H and 4% 6H. Comparing this to our combinatorial model, if we assume growth conditions so that $p_h > 1/2$ and fix $p_{4H} = 7\%$ as in Figure 3a, we get $p_{6H} = 6\%$ according to eq 1. This corresponds to $p_h = 0.75$. Correspondingly, if $p_{4H} = 4\%$ as in Figure 3b we get $p_{6H} = 3\%$, corresponding to $p_h = 0.83$. These high values of p_h are qualitatively consistent with the high supersaturation growth conditions of the parts of the nanowires shown in Figure 3. The influences of growth parameters and materials properties on p_c and p_h are outlined in the Methods section. Considering statistical fluctuations and the difficulty to characterize the crystal structure from the HRTEM images in an unambiguous way, the correspondence between theory and experiment is good.

Mariager *et al.*[13] used X-ray diffraction (XRD) to study the facets and crystal structure of GaAs nanowires and showed that parts of the nanowires contained extended but rare portions of a crystal segment referred to as "type 6", later identified as 6H. It is interesting to note that Mariager *et al.* report 6H and not 4H. This is in line with our model, where 4H never dominates and is less probable than 6H for most conditions.

Tomioka *et al.*[28] report on the crystal structure of selective area MOVPE-grown InAs nanowires. The structure of these wires appears to be a quasi-periodic mixture of irregularly stacked 4H and 6H, in qualitative agreement with the combinatorial model. A similar crystal structure in InAs nanowires was observed by Koguchi *et al.*[29]

Although experimental findings lend credibility to our combinatorial model, it cannot explain the long segments of different polytypes in the same nanowire, nor the abundance of the 4H polytype reported during the last couple of years.[13−17] These reports, where extended segments of 3C, 4H, and 2H are observed, seem to be qualitatively different than the results described above and suggest that there is a longer range order in the crystal structure than what can be explained by the combinatorial model alone. This suggests that there can be significant interlayer interactions in nanowires, and to address this, we consider the axial next nearest neighbor Ising (ANNNI) model.[30] A good description of the ANNNI model and its application to polytypism in SiC is given in ref 31. In brief, a stacking sequence is treated as analogous to a sequence of generalized spins, and the total energy, E, of a system consisting of N stacked layers can be written as

$$E = E_0 - \frac{1}{N}\sum_{i,n} J_n s_i s_{i+n} \quad (2)$$

where E_0 is the energy of the crystal if there were no interaction between the layers, J_n is the interaction energy between the nth neighboring layers, and the generalized spin is $s_i = +1$ (also denoted by ↑) or -1 (↓), depending on which layer, layer i was stacked. The value of $s_i = +1$ if layer i on layer $i-1$ is any one of the combinations B on A, C on B, and A on C. For the three other combinations, that is the reversed stacking order, $s_i = -1$.

We use the ANNNI model to estimate the interface energy, σ_i (see Methods section), associated with nucleation of a specifically stacked nucleus on a specific sequence of layers. We consider interactions of the nucleating layer with up to next nearest neighbor, corresponding to $i = 1$ and $n = 1$ to 2 in eq 2. That is, as a first approximation we ignore the J_3 term. The interface energy term, which is the extra energy per surface area for adding a new layer on top of an existing sequence of layers, is calculated from[32]

$$\sigma_i = \sigma_0 - J_1 s_1 s_2 - J_2 s_1 s_3 \quad (3)$$

where the subscript i denotes the polytype, σ_0 is a reference value for the interface energy, and J_1 and J_2 are the strengths of the interactions between the nucleating layer and its nearest and next nearest neighboring layer, respectively.

In order to avoid one additional free parameter (J_3) and problems with stacking sequence truncation, we restrict the interlayer interaction approach to polytypes up to 4H. To describe these, we need to include four layers in the analysis. The stacking sequence for 3C is represented by all generalized spins in the same direction. Thus, in order to create four layers of 3C, two identical consecutive nucleation events of type ↑-on-↑↑ with probabilities p_{3C} are needed. The 4H polytype is represented by pairs of parallel generalized spins, every other pair up and every other pair down. In order to create four layers of this polytype, one nucleation event of type ↑-on-↓↓, with probability $p_{4H'}$ followed one nucleation event of type ↑-on-↑↓, with probability $p_{4H''}$, has to occur, or *vice versa*. Finally, in order to create four layers of 2H, two identical consecutive nucleation events of type ↑-on-↓↑ with probabilities p_{2H} are needed. These p_i's are all given by ratios of nucleation rates, as described in the Methods section.

Following the model calculation for polytypism in SiC we let $J_1 > 0$ and $J_2 < 0$ and we set $J_1/J_2 = -\eta$ with η positive.[31] As the twin plane energy, σ_t, is known for many III−V semiconductors, the σ_i's are expressed in terms of σ_t, which is given by $\sigma_t = 2J_1 + 4J_2$.[33] Since 4H″ is the most energetically favorable type of stacking,

we set $\sigma_{4H''} = 0$. This leads to

$$\begin{aligned}\sigma_{3C} &= \sigma_t \frac{1}{\eta - 2} \\ \sigma_{4H'} &= \sigma_t \frac{\eta}{\eta - 2} \\ \sigma_{4H''} &= 0 \\ \sigma_{2H} &= \sigma_t \frac{\eta + 1}{\eta - 2}\end{aligned} \quad (4)$$

We see that for all $\eta > 2$ the inequalities $\sigma_{4H''} < \sigma_{3C} < \sigma_{4H'} < \sigma_{2H}$ are always satisfied, which should be required for materials with 3C as bulk crystal structure. If $\eta = 0$, J_2 is much more significant than J_1 and 4H is suppressed in favor of 2H and 3C. If $\eta \rightarrow \infty$, J_1 is much more significant than J_2 and $\sigma_{2H} \rightarrow \sigma_t$ and $\sigma_{3C} \rightarrow 0$ as in the combinatorial model. Based on these observations, an η in the range 2–10 we believe is realistic for many metal particle–nanowire materials systems. This range has the same magnitude as the values calculated by Panse *et al.*[34] For this choice of η the formation of 2H is not suppressed, while J_2 is still significant compared to J_1.

The interface energy, σ_i, is one of the two properties that are used to distinguish between polytypes in the current model. We also need the step energies, Γ_i, of the different polytypes. In accordance with our previous nucleation modeling (see Methods section), we set the step energy of the interior of the nuclei, γ_0, equal to the edge step energy of 3C, $\gamma_0 = \gamma_{3C}$.[22,25] Since the step energies are expected to follow the same trends as the surface energies, we expect the edge step energy of 2H to be smaller than that for 3C.[35–37] In addition, since 4H′ stacking is identical to 2H stacking if we only consider nearest neighboring layers, we will make the approximation $\gamma_{4H'} = \gamma_{2H}$. For the same reason we will set $\gamma_{4H''} = \gamma_{3C}$.

We can now calculate the formation probabilities for the polytypes 3C, 4H, and 2H,

$$\begin{aligned}\rho_{3C} &= \frac{p_{3C}^2}{p_{3C}^2 + 2p_{4H'}p_{4H''} + p_{2H}^2} \\ \rho_{4H} &= \frac{2p_{4H'}p_{4H''}}{p_{3C}^2 + 2p_{4H'}p_{4H''} + p_{2H}^2} \\ \rho_{2H} &= \frac{p_{2H}^2}{p_{3C}^2 + 2p_{4H'}p_{4H''} + p_{2H}^2}\end{aligned} \quad (5)$$

In Figure 4 we plot an example of ρ_{3C}, ρ_{4H}, and ρ_{2H} as given by eq 5 as functions of supersaturation for gold-seeded GaAs nanowire growth. The nucleation probability of a certain polytype is a good approximation of the relative occurrence of that polytype in a nanowire, and the trend shown in Figure 4 is that 3C is favored at low supersaturation, 4H is favored at intermediate

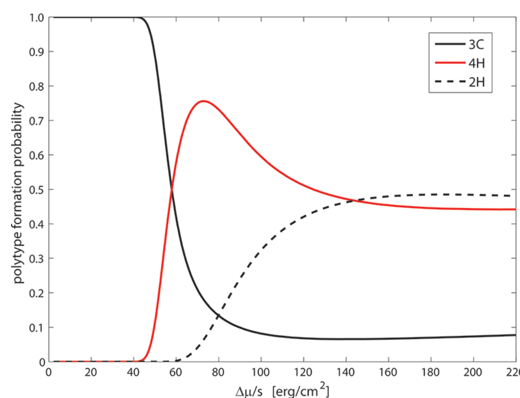

Figure 4. Polytype formation probability for 3C, 4H, and 2H as a function of supersaturation (measured as chemical potential difference) calculated for gold particle seeded GaAs nanowire growth. We use the following parameters: lattice constant $a = 5.65 \times 10^{-8}$ cm, step energy $\gamma_{3C} = 119.3$ erg/cm^3,[49] and twin plane energy $\sigma_t = 22.5$ erg/cm^2.[49] We chose a growth temperature of $T = 500$ °C and an interaction range parameter $\eta = 8$. As edge step energies we use $\gamma_{2H}/\gamma_{3C} = \gamma_{4H'}/\gamma_{3C} = 0.4$.

supersaturation, and 2H is favored at high supersaturation. In addition, the formation probability of 4H is still quite high in comparison with 2H at high supersaturation, indicating that it can be difficult to achieve defect-free 2H nanowires without any inclusions of stacking faults or short segments of 4H. Note that with the purely combinatorial model discussed previously it is also more difficult to achieve defect-free 2H than defect-free 3C.

We now compare predictions made from the model based on ANNNI to experimental results found for Sb-based materials, where several reports show the presence of 4H. In this materials system, different research groups have reported on changes in the crystal structure along the nanowires and proposed changes in supersaturation as a possible explanation. In Figure 5, HRTEM images of gold particle seeded, molecular beam epitaxy (MBE)-grown $InAs_{1-x}Sb_x$/InAs nanowire heterostructures are displayed. The lower and upper part of the structure contains Sb and has the 3C structure (Figure 5a). After the Sb source is turned off, a short segment of the 3C structure forms, followed by an intermediate segment 4H, followed by 2H (Figure 5b). Under the growth conditions used here, InAs is normally pure wurtzite,[38] while InAsSb becomes pure zinc blende if the Sb content is high enough.[39]

These results are fully consistent with the results of Dheeraj *et al.*[14] They report MBE growth of gold particle seeded $GaAs_{1-x}Sb_x$/GaAs nanowire heterostructures, where the GaAs segments had 2H structure, GaAsSb segments had the 3C structure, and extended segments of 4H were found at the transition. Dheeraj *et al.* proposed a model where 4H is considered to be an intermediate crystal structure between 3C and 2H, forming at intermediate supersaturation.

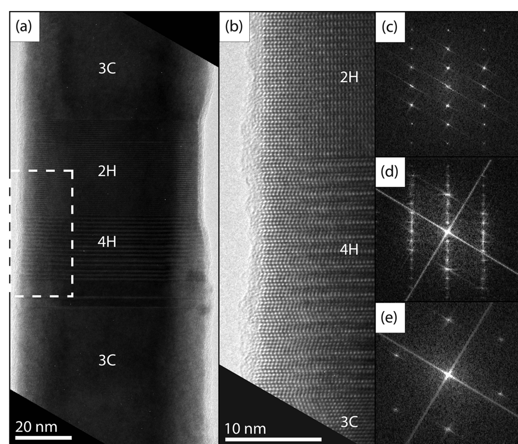

Figure 5. TEM images along a ⟨1−10⟩ zone axis of part of an $InAs_{1-x}Sb_x$/InAs heterostructure nanowire showing the transition from 3C to 2H *via* an extended segment of 4H after the Sb_2 flux is shut off. Since residual Sb can remain on the nanowire sidewalls, and in the seed particle after the Sb_2 flux is shut off, this gradual structural transition can occur. When the Sb_2 flux is turned on again, the crystal structure changes to 3C. (a) Overview of a nanowire. (b) HRTEM image of part of the nanowire in (a) (the region indicated by the dashed frame). The regions of 3C, 4H,and 2H are indicated. Diffractograms calculated from high-resolution images of the segments shown in (a) and partly in (b) are shown for (c) 2H, (d) 4H, and (e) for 3C.

In both these investigations the Sb-containing segments exhibit the 3C polytype. A plausible explanation for this is that the Sb increases the equilibrium concentration of the group III species (In or Ga) in the gold particle compared to arsenide and phosphide systems,[40,41] in turn decreasing the supersaturation. When the Sb source is turned off, the excess Sb in the alloy particle is consumed, decreasing group III solubility and increasing supersaturation. The crystal structure then changes from 3C at low supersaturation to 4H and finally to 2H at high supersaturation, according to the model illustrated in Figure 4. This hypothesis is further strengthened by the results of Mandl *et al.*[16] They observed that gold-free InSb nanowires grown with MOVPE evolved from the 3C crystal structure to 2H *via* extended segments of 4H. The authors explained the phase change by an increased Sb concentration in the In−Sb seed particle, which likely results in a supersaturation high enough for the formation of 4H and 2H.

The reason for the several reports of 4H in Sb-based materials is probably longer range interlayer interactions in these materials compared to Sb-free materials in general. Panse *et al.*[34] have calculated the interaction parameters J_1, J_2, and J_3 for InSb, GaAs, InAs, InP, and SiC. They found that J_3/J_2 indeed is highest for InSb, which is consistent with the experimental trend.

In our model, where we omit J_3, the interlayer interaction range is instead measured by $\eta = |J_1/J_2|$. By increasing η, the formation probability of 4H is decreasing. Thus, by use of a higher value of η as compared to the value used in Figure 4, the model should be applicable also to materials where extended regions of 4H are rarer, such as GaAs and InAs.

On the other hand, if η is lowered, the formation probability of 4H increases, and in order to include even higher polytypes, higher order interaction parameters must be included in the analysis. To include polytypes up to 6H, the parameter J_3 is required, and the stability window for 6H has been reported to widen as J_3 is increased.[31,34]

CONCLUSIONS

In conclusion, we have proposed two models for the polytypism in III−V nanowires. Both approaches go beyond the well-investigated zinc blende−wurtzite (3C−2H) polytypism,[23−26,37,42−44] to include the 4H and 6H polytypes.

Our first model is purely combinatorial, and we include polytypes up to 6H. This model predicts that at low and high probability for hexagonal stacking the polytypes 3C and 2H, respectively, dominate, which is consistent with experimental investigations.[10] Moreover, there is an interval of moderate hexagonal stacking probability where 6H dominates, and a striking result is that 4H never dominates. These results compare qualitatively with experimental results on nanowires with mixed crystal structure, lacking long-range order.

On the other hand, in many other nanowire systems the crystal structure has a longer range order and extended segments of 3C, 2H, and 4H are observed. A second approach we make is therefore to explicitly include interlayer interactions beyond nearest neighbor to express the formation probabilities of these polytypes. The trends predicted by this model compare well with experimental results on Sb-based nanowires. It is interesting to note that both models indicate that it could be more difficult to get defect-free 2H than defect-free 3C.

We are convinced that these results will pave the way for future research on controlled fabrication of not only 2H and 3C but also higher polytypes, such as 4H and 6H, in III−V nanowires, significantly adding design freedom for nanowire-based devices.

METHODS

Classical Nucleation Modeling. Here we will relate experimentally controllable parameters and materials properties to the probability for a certain kind of stacking based on the classical nucleation framework outlined in detail in refs 25 and 26. The probability for stacking sequence i (i = h or c) is denoted by p_i and is given by the ratio of nucleation rates, $p_i = I_i/\Sigma I_i$ where I_i is the nucleation rate for stacking sequence i, and the summation

goes over all possible types of nuclei. The nucleation rate can in turn be expressed as $I_i = \omega^* n Z_i \exp(-\Delta G^*_i/k_B T)$, where ω^* is the attachment frequency of building blocks to the critical nucleus, n is the concentration of the limiting species in the alloy particle, and Z_i is the Zeldovich factor, which is a slowly varying function given explicitly in ref 26. The exponent contains the barrier for nucleation in stacking sequence i and the thermal energy $k_B T$. The energy barrier, ΔG^*_i, can be expressed as $\Delta G^*_i = \Gamma_i^2/(2\pi[\Delta\mu/s - \sigma_i])$, where Γ_i is the step energy, $\Delta\mu$ is the difference in chemical potential between the growth species in the seed particle and in the nanowire,[26] s is the area of a molecular site, and σ_i is an interface energy that accounts for the increase in interfacial energy per area unit by forming a type i nucleus. The step energy can be written as $\Gamma_i = (2\gamma_i + \pi\gamma_0)h$, where γ_i is the specific step energy of the edge part of nucleus i and γ_0 is the step energy of the interior part of the nucleus, which we will take to be the same for all considered types of nuclei.

There are at least three parameters that influence the layer stacking and consequently the polytypism in nanowires: $\Delta\mu$, Γ_i, and σ_i. The difference in chemical potential, $\Delta\mu$, is an experimentally attainable parameter and can be controlled by the precursor fluxes,[25,45,46] by the size of the metal particle,[26] and, if feasible, by experimentally changing the solubility properties of the metal particle.[25] A high value of $\Delta\mu$ favors hexagonal stacking. The step energy, Γ_i, is a materials parameter that is believed to follow the same trend as the surface energy does. That is, 2H has lower surface energies than 3C, when comparing corresponding surfaces in the same material.[35−37] From this follows that Γ_i generally decreases with increasing hexagonality. The interface energy, σ_i, accounts for the increase in interface energy for a certain stacking sequence. Generally σ_i increases with increasing hexagonality, and in the combinatorial model we use $\sigma_c = 0$ and $\sigma_h = \sigma_t$, the twin plane energy.[22]

To conclude, the formation of hexagonal polytypes is favored if there is a high enough supersaturation of precursor atoms in the seed particle and if the edge step energies decrease with increasing hexagonality. These two necessary conditions seem quite robust and are fulfilled for III−V nanowire growth with most epitaxial techniques, such as MOVPE, MBE, and gas source MBE. The interface energies for the different polytypes depend on the materials system only (semiconductor−seed metal combination). Evaluations of the experimental parameter dependencies of nanowire crystal structures are given in refs 43, 47, 48, and 10.

Epitaxial Growth. The GaAs nanowires were grown by low-pressure metal organic vapor phase epitaxy using gold nanoparticles as seeds. Gold aerosol nanopartices with a diameter of 50 nm were deposited onto epi-ready Si-doped (111)B oriented GaAs substrates. A pregrowth annealing step was employed, involving annealing of the particle spread substrates at 650 °C for about 5 min in a background of arsine (AsH_3), and the nanowires were grown by using a two-temperature scheme: After the annealing the temperature was decreased to 440 °C and nanowire growth was initiated by supplying trimethyl gallium (TMG). After 12 min the TMG supply was turned off and the temperature was increased to either 630 or 690 °C. Growth was then reinitiated by supplying TMG for 3 min. Growth was finished by turning off the TMG supply and cooling the samples to room temperature. The AsH_3 supply was kept throughout the growth process from the start of the pregrowth annealing step until the samples had reached a temperature below 300 °C during the cooling step in the very end of the growth process. Molar fractions of 9×10^{-6} and 9×10^{-4} for TMG and AsH_3, respectively, were used, giving a nominal V/III ratio of 100.

Gold particle assisted $InAs/InAs_{1-x}Sb_x$ superlattice heterostructure nanowires were grown by gas source molecular beam epitaxy on InP(111)B substrates. Gold droplets were obtained by standard dewetting of a 3 Å gold film (evaporated *ex situ*), during the pregrowth deoxidation and annealing step at 525 °C. After this, the temperature was decreased and the growth was initiated at 410 °C by an InP nanowire stem grown for 20 min, followed by an InAs stem grown for 25 min, using V/III ratios set to around 2.0 for both InP and InAs. A first extended InAsSb segment is grown for 3 min, followed by an InAs segment grown for 2 min as marker layers directly before the superlattice. The superlattice, consisting of 10 segments of InAsSb in InAs, is then finally obtained by periodically opening the Sb shutter for 45 s (growth of $InAs_{1-x}Sb_x$) and shutting it off for 60 s (growth of InAs segments). No growth interruption sequence is used at interfaces. The antimony flux was adjusted to correspond to an average antimony fraction of about 0.2, measured by energy-dispersive spectroscopy in point-scan analysis mode.

TEM Characterization. Samples were prepared by direct transfer of the nanowires (NWs) to a lacey carbon Cu grid by gently pressing the grid to the substrate. High-resolution images were acquired along the entire high-temperature growth section in a ⟨110⟩ projection for several NWs from each sample using a 300 kV Jeol TEM.

The fractions of the higher order polytypes 4H and 6H were calculated from the summed lengths for segments of each type divided by the total length of the NW section containing hexagonal stacking (excluding the low-*T*-grown stem and the tip formed during cool down, both of which are pure zinc blende). In order to only include the higher order polytypes (*e.g.*, to exclude a short twin in a zinc blende segment) in the calculated fractions and to make the 4H and 6H fractions comparable, only segments longer than 12 ML were included, *i.e.*, three and two unit cells, respectively.

The atomic models displayed in Figure 1 were made with the software ATOMS.

Conflict of Interest: The authors declare no competing financial interest.

Acknowledgment. This work was performed within the Nanometer Structure Consortium at Lund University (nmC@LU) and within the Institute for Electronics, Microelectronics and Nanotechnology, Centre National de la Recherche Scientifique (IEMN, UMR CNRS 8520). The samples were fabricated both in LundNanoLab and in IEMN; the TEM characterization was done at the Swedish National Center for High Resolution Electron Microscopy (nCHREM). We acknowledge funding from the nmC@LU, the Swedish Research Council (VR), the Swedish Foundation for Strategic Research (SSF), and the Knut and Alice Wallenberg Foundation (KAW).

REFERENCES AND NOTES

1. Fan, H. J.; Werner, P.; Zacharias, M. Semiconductor Nanowires: From Self-Organization to Patterned Growth. *Small* **2006**, *2*, 700–717.
2. Kolasinski, K. W. Catalytic Growth of Nanowires: Vapor-Liquid-Solid, Vapor-Solid-Solid, Solution-Liquid-Solid and Solid-Liquid-Solid Growth. *Curr. Opin. Solid State Mater. Sci.* **2006**, *10*, 182–191.
3. Lu, W.; Lieber, C. M. Semiconductor Nanowires. *J. Phys. D Appl. Phys.* **2006**, *39*, R387–R406.
4. Dick, K. A. A Review of Nanowire Growth Promoted by Alloys and non-Alloying Elements with Emphasis on Au-Assisted III-V Nanowires. *Prog. Cryst. Growth Charact. Mater.* **2008**, *54*, 138–173.
5. Yang, P. D.; Yan, R. X.; Fardy, M. Semiconductor Nanowire: What's Next? *Nano Lett.* **2010**, *10*, 1529–1536.
6. Wernersson, L. E.; Thelander, C.; Lind, E.; Samuelson, L. III-V Nanowires-Extending a Narrowing Road. *Proc. IEEE* **2010**, *98*, 2047–2060.
7. Yan, R. X.; Gargas, D.; Yang, P. D. Nanowire Photonics. *Nat. Photonics* **2009**, *3*, 569–576.
8. Patolsky, F.; Zheng, G.; Lieber, C. M. Nanowire Sensors for Medicine and the Life Sciences. *Nanomedicine* **2006**, *1*, 51–65.
9. Heiss, M.; Conesa-Boj, S.; Ren, J.; Tseng, H. H.; Gali, A.; Rudolph, A.; Uccelli, E.; Peiro, F.; Morante, J. R.; Schuh, D.; *et al.* Direct Correlation of Crystal Structure and Optical Properties in Wurtzite/Zinc-Blende GaAs Nanowire Heterostructures. *Phys. Rev. B* **2011**, *83*, 045303.
10. Caroff, P.; Bolinsson, J.; Johansson, J. Crystal Phases in III−V Nanowires: From Random Toward Engineered Polytypism. *IEEE J. Sel. Top. Quantum Electron.* **2011**, *17*, 829–846.

11. Ramsdell, L. S. Studies on Silicon Carbide. *Am. Mineral.* **1947**, *32*, 64–82.
12. Davidson, F. M.; Lee, D. C.; Fanfair, D. D.; Korgel, B. A. Lamellar Twinning in Semiconductor Nanowires. *J. Phys. Chem. C* **2007**, *111*, 2929–2935.
13. Mariager, S. O.; Sorensen, C. B.; Aagesen, M.; Nygård, J.; Feidenhans'l, R.; Willmott, P. R. Facet Structure of GaAs Nanowires Grown by Molecular Beam Epitaxy. *Appl. Phys. Lett.* **2007**, *91*, 083106.
14. Dheeraj, D. L.; Patriarche, G.; Zhou, H. L.; Hoang, T. B.; Moses, A. F.; Gronsberg, S.; van Helvoort, A. T. J.; Fimland, B. O.; Weman, H. Growth and Characterization of Wurtzite GaAs Nanowires with Defect-Free Zinc Blende GaAsSb Inserts. *Nano Lett.* **2008**, *8*, 4459–4463.
15. Soshnikov, I. P.; Cirlin, G. E.; Sibirev, N. V.; Dubrovskii, V. G.; Samsonenko, Y. B.; Litvinov, D.; Gerthsen, D. Hexagonal Structures in GaAs Nanowhiskers. *Tech. Phys. Lett.* **2008**, *34*, 538–541.
16. Mandl, B.; Dick, K. A.; Kriegner, D.; Keplinger, M.; Bauer, G.; Stangl, J.; Deppert, K. Crystal Structure Control in Au-Free Self-Seeded InSb Wire Growth. *Nanotechnology* **2011**, *22*, 145603.
17. Kriegner, D.; Panse, C.; Mandl, B.; Dick, K. A.; Keplinger, M.; Persson, J. M.; Caroff, P.; Ercolani, D.; Sorba, L.; Bechstedt, F.; *et al.* Unit Cell Structure of Crystal Polytypes in InAs and InSb Nanowires. *Nano Lett.* **2011**, *11*, 1483–1489.
18. Algra, R. E.; Verheijen, M. A.; Borgström, M. T.; Feiner, L. F.; Immink, G.; van Enckevort, W. J. P.; Vlieg, E.; Bakkers, E. P. A. M. Twinning Superlattices in Indium Phosphide Nanowires. *Nature* **2008**, *456*, 369–372.
19. Caroff, P.; Dick, K. A.; Johansson, J.; Messing, M. E.; Deppert, K.; Samuelson, L. Controlled Polytypic and Twin-Plane Superlattices in III-V Nanowires. *Nat. Nanotechnol.* **2009**, *4*, 50–55.
20. Algra, R. E.; Hocevar, M.; Verheijen, M. A.; Zardo, I.; Immink, G. G. W.; van Enckevort, W. J. P.; Abstreiter, G.; Kouwenhoven, L. P.; Vlieg, E.; Bakkers, E. P. A. M. Crystal Structure Transfer in Core/Shell Nanowires. *Nano Lett.* **2011**, *11*, 1690–1694.
21. Bolinsson, J. The Crystal Structure of III-V Semiconductor Nanowires: Growth and Characterization. Ph.D. Thesis, Lund University, Lund, 2010.
22. Johansson, J.; Karlsson, L. S.; Svensson, C. P. T.; Mårtensson, T.; Wacaser, B. A.; Deppert, K.; Samuelson, L.; Seifert, W. Structural Properties of (111)B-Oriented III-V Nanowires. *Nat. Mater.* **2006**, *5*, 574–580.
23. Glas, F.; Harmand, J. C.; Patriarch, G. Why Does Wurtzite Form in Nanowires of III-V Zinc Blende Semiconductors? *Phys. Rev. Lett.* **2007**, *99*, 146101.
24. Akiyama, T.; Sano, K.; Nakamura, K.; Ito, T. An Empirical Potential Approach to Wurtzite-Zinc-Blende Polytypism in Group III-V Semiconductor Nanowires. *Jpn. J. Appl. Phys.* **2006**, *45*, L275–L278.
25. Johansson, J.; Karlsson, L. S.; Dick, K. A.; Bolinsson, J.; Wacaser, B. A.; Deppert, K.; Samuelson, L. Effects of Supersaturation on the Crystal Structure of Gold Seeded III-V Nanowires. *Cryst. Growth Des.* **2009**, *9*, 766–773.
26. Johansson, J.; Dick, K. A.; Caroff, P.; Messing, M. E.; Bolinsson, J.; Deppert, K.; Samuelson, L. Diameter Dependence of the Wurtzite-Zinc Blende Transition in InAs Nanowires. *J. Phys. Chem. C* **2010**, *114*, 3837–3842.
27. Verma, A. R.; Krishna, P. *Polymorphism and Polytypism in Crystals*, 1st ed.; John Wiley & Sons: New York, 1966.
28. Tomioka, K.; Motohisa, J.; Hara, S.; Fukui, T. Crystallographic Structure of InAs Nanowires Studied by Transmission Electron Microscopy. *Jpn. J. Appl. Phys.* **2007**, *46*, L1102–L1104.
29. Koguchi, M.; Kakibayashi, H.; Yazawa, M.; Hiruma, K.; Katsuyama, T. Crystal Structure Change of GaAs and InAs Whiskers from Zinc-Blende to Wurtzite Type. *Jpn. J. Appl. Phys.* **1992**, *31*, 2061–2065.
30. Boehm, J. V.; Bak, P. Devils Stairs and the Commensurate-Commensurate Transitions in CeSb. *Phys. Rev. Lett.* **1979**, *42*, 122–125.
31. Cheng, C.; Needs, R. J.; Heine, V. Inter-Layer Interactions and the Origin of SiC Polytypes. *J. Phys. C* **1988**, *21*, 1049–1063.
32. Heine, V.; Cheng, C.; Needs, R. J. The Preference of Silicon-Carbide for Growth in the Metastable Cubic Form. *J. Am. Ceram. Soc.* **1991**, *74*, 2630–2633.
33. Limpijumnong, S.; Lambrecht, W. R. L. Total Energy Differences between SiC Polytypes Revisited. *Phys. Rev. B* **1998**, *57*, 12017–12022.
34. Panse, C.; Kriegner, D.; Bechstedt, F. Polytypism of GaAs, InP, InAs, and InSb: An Ab Initio Study. *Phys. Rev. B* **2011**, *84*, 075217.
35. Zhang, H. Z.; Huang, F.; Gilbert, B.; Banfield, J. F. Molecular Dynamics Simulations, Thermodynamic Analysis, and Experimental Study of Phase Stability of Zinc Sulfide Nanoparticles. *J. Phys. Chem. B* **2003**, *107*, 13051–13060.
36. Dubrovskii, V. G.; Sibirev, N. V. Growth Thermodynamics of Nanowires and its Application to Polytypism of Zinc Blende III-V Nanowires. *Phys. Rev. B* **2008**, *77*, 035414.
37. Yamashita, T.; Akiyama, T.; Nakamura, K.; Ito, T. Theoretical Investigation on the Structural Stability of GaAs Nanowires with Two Different Types of Facets. *Phys. E* **2010**, *42*, 2727–2730.
38. Thelander, C.; Caroff, P.; Plissard, S.; Dey, A. W.; Dick, K. A. Effects of Crystal Phase Mixing on the Electrical Properties of InAs Nanowires. *Nano Lett.* **2011**, *11*, 2424–2429.
39. Xu, T.; Dick, K. A.; Plissard, S.; Nguyen, T. H.; Makoudi, Y.; Berthe, M.; Nys, J.-P.; Wallart, X.; Grandidier, B.; Caroff, P. Faceting, Composition and Crystal Phase Evolution in III−V Antimonide Nanowire Heterostructures Revealed by Combining Microscopy Techniques. *Nanotechnology* **2012**, *23*, 095702.
40. Tsai, C. T.; Williams, R. S. Solid Phase Equilibria in the Au-Ga-As, Au-Ga-Sb, Au-In-As, and Au-In-Sb ternaries. *J. Mater. Res.* **1986**, *1*, 352–360.
41. Caroff, P.; Wagner, J. B.; Dick, K. A.; Nilsson, H. A.; Jeppsson, M.; Deppert, K.; Samuelson, L.; Wallenberg, L. R.; Wernersson, L. E. High-Quality InAs/InSb Nanowire Heterostructures Grown by Metal-Organic Vapor-Phase Epitaxy. *Small* **2008**, *4*, 878–882.
42. Dubrovskii, V. G.; Sibirev, N. V.; Harmand, J. C.; Glas, F. Growth Kinetics and Crystal Structure of Semiconductor Nanowires. *Phys. Rev. B* **2008**, *78*, 235301.
43. Joyce, H. J.; Wong-Leung, J.; Gao, Q.; Tan, H. H.; Jagadish, C. Phase Perfection in Zinc Blende and Wurtzite III-V Nanowires Using Basic Growth Parameters. *Nano Lett.* **2010**, *10*, 908–915.
44. Krogstrup, P.; Curiotto, S.; Johnson, E.; Aagesen, M.; Nygard, J.; Chatain, D. Impact of the Liquid Phase Shape on the Structure of III-V Nanowires. *Phys. Rev. Lett.* **2011**, *106*, 125505.
45. Bolinsson, J.; Caroff, P.; Mandl, B.; Dick, K. A. Wurtzite-Zincblende Superlattices in InAs Nanowires Using a Supply Interruption Method. *Nanotechnology* **2011**, *22*, 265606.
46. Mohseni, P. K.; LaPierre, R. R. A Growth Interruption Technique for Stacking Fault-Free Nanowire Superlattices. *Nanotechnology* **2009**, *20*, 025610.
47. Dick, K. A.; Caroff, P.; Bolinsson, J.; Messing, M. E.; Johansson, J.; Deppert, K.; Wallenberg, L. R.; Samuelson, L. Control of III-V Nanowire Crystal Structure by Growth Parameter Tuning. *Semicond. Sci. Technol.* **2010**, *25*, 024009.
48. Dick, K. A.; Bolinsson, J.; Messing, M. E.; Lehmann, S.; Johansson, J.; Caroff, P. Parameter Space Mapping of InAs Nanowire Crystal Structure. *J. Vac. Sci. Technol. B* **2011**, *29*.
49. Hurle, D. T. J. A Mechanism for Twin Formation During Czochralski and Encapsulated Vertical Bridgeman Growth of III-V Compound Semiconductors. *J. Cryst. Growth* **1995**, *147*, 239–250.